RESEARCH PAPER

PCCP
www.rsc.org/pccp

Viscoelastic and small angle neutron scattering studies of concentrated protein solutions†

B. Lonetti,[a] E. Fratini,[a] S. H. Chen[b] and P. Baglioni*[ab]

[a] *Department of Chemistry and CSGI, University of Florence, 50019 Sesto Fiorentino, Italy. E-mail: baglioni@csgi.unifi.it; Fax: +39 055 457 3032*

[b] *Department of Nuclear Engineering, Massachusetts Institute of Technology, Cambridge 02139, Massachusetts, USA*

Received 10th December 2003, Accepted 4th February 2004
First published as an Advance Article on the web 5th March 2004

Small angle neutron scattering (SANS) and rheological measurements have been used to study horse heart cytochrome C, a globular protein characterized by approximately spherical shape ($a \times b \times b = 15 \times 17 \times 17$ Å^3) with a molecular weight of 12 384 Da and a pI = 10.2. Two series of very concentrated protein solutions have been investigated at pD 5.4 and 11.0, respectively, the volume fraction of the protein spanning from 0.1 to 0.5. The Krieger–Dougherty model was applied to describe the relation between relative high shear viscosity of the solution and volume fraction of the protein at both pD in order to elucidate the charge effect on the interaction potential. The SANS intensity distributions at pD 5.4 were fitted using the GOCM model with an excellent agreement between the theory and experiments up to the volume fraction ϕ of 0.4. At pD 11.0 the intensity distribution at $\phi = 0.1$ can be fitted with a pure form factor (oblate ellipsoid), suggesting that under this condition the cytochrome C molecules are almost uncharged and preserve the native molecular size. Addition of salt induces the transformation from liquid to a gel. This is a result of formation of ordered fractal clusters internally as evident from appearance of a second interaction peak at very low Q (magnitude of the scattering vector). The appearance of the low Q peak is also accompanied by a strong increase in the relative viscosity. These phenomena taken together can be considered as the signature of the gelation process.

Introduction

Proteins play a critical role in almost all biological processes, and the understanding of the physical basis of their mutual interactions is a key to this understanding. In order to develop a model that describes the interactions among biological macro-ions leading to a general theory of liquid-crystal transition, it is essential to have a clear picture of the forces acting among proteins in solution.[1,2]

Surface charge and inter-particle interactions of globular proteins can be easily modulated by varying pH, salt concentration and temperature. Protein solutions are stable when Coulombic repulsions dominate the attractive interactions. At the isoelectric point, pI, the number of positively charged groups equals the number of negatively charged ones and the protein solubility drastically drops with formation of amorphous precipitates.[3–5] In order to overcome this inconvenience some repulsive contributions at the interactions potential have to be preserved. This is typically obtained by using a pH far from the isoelectric point and adding a salt whose counter-ions partially screen the charges on the proteins. The optimal crystallization conditions are strongly linked with a salt concentration able to reduce the range of electrostatic repulsions at distances where the attractive forces are effective (*i.e.* the Debye length is shorter than macro-ion diameter). A very intriguing effect is the so-called 'Hofmeister anion effect':[6] in fact different salts at the same ionic strength produce different effects on the weak balance between attractive and repulsive forces. The complexity of this phenomenon is evident: protein concentration, temperature, pH, ionic strength and nature of the added salt and kinetic aspects have to be taken into account when trying to obtain good protein crystals.

The easiest way to relate easily measurable solution properties with crystallization conditions is to assimilate proteins to colloidal particles hence using their well-known models. George and Wilson[7] studied under-saturated lysozyme solutions in crystallization condition. They employed the static light scattering to determine the sign and magnitude of the virial coefficient, B, thus characterizing concretely the net interaction. In all cases, negative values of B were obtained. Muschol and Rosenberger extended previous studies to lysozyme solutions in conditions of over-saturation[8–10] confirming that the virial coefficient, B, must be negative in order to have optimal crystallization conditions. Both these approaches were based on the DLVO[11,12] description of the intermolecular interactions. Furthermore, Piazza *et al.*[13,14] and Rosenbaum *et al.*[15] modeled protein solutions as adhesive hard sphere (AHS) systems in which the interaction potential is made up of a repulsive core plus a short range attractive tail.

Lysozyme and cytochrome C are excellent model systems since their shape is globular and very close to a sphere. Due to the strong absorbance at 410 nm the cytochrome C cannot be studied by light scattering as usually happens with lysozyme. However, cytochrome C solution properties are accessible by using small angle neutron and X-ray scattering techniques (SANS, SAXS), even though the information obtained by these latter techniques cover a smaller length scale range.

Wu *et al.* adopted another effective approach to the problem of protein interactions. They performed SANS and SAXS experiments on cytochrome C in aqueous solutions up to volume fractions ϕ of about 0.18.[16,17] They analyzed the SANS and SAXS data using the generalized one-component macro-ion (GOCM) theory,[17] an extension of the well-known

† Presented at the 17th Conference of the European Colloid & Interface Science Society, Firenze, Italy, September 21–26, 2003.

DOI: 10.1039/b316144g

one-component macro-ion model (OCM),[18] which is applicable at high volume fractions. Using this model, they extracted some protein parameters at different pD values: the hydrated diameter, the amount of hydration, the degree of H/D exchange with the solvent and the renormalized charge. Besides, they compared the renormalized charge obtained through the fitting procedure with the charge measured by conventional titration experiments and found good agreement at intermediate pD values, *i.e.* at pD = 6.8.[16] However, at extreme pD values (*i.e.* 2.9 and 11.9) they obtained the renormalized charge significantly lower than the titration charge and attributed this discrepancy to the so-called charge renormalization phenomenon.[17] Microscopically, this can be explained as the result of a piling up of counter-ions near the protein surface, the analogue of the charge condensation phenomenon in rod-like particles such as DNA. Thus, as far as the protein–protein interactions are concerned, counter-ions behave like a part of the protein itself. Regardless of the charge renormalization phenomenon, the essential point of their work is that they were able to relate the results of scattering experiments to the thermodynamic properties of the protein solutions.

In this paper we extended previous studies[16,17] to the investigation of concentrated cytochrome C solutions. Two limiting cases were taken into account: a series at pD 5.4 exhibiting long-range repulsion and a very weak attractive interaction and a series at pD 11.0 where the short-range attractions are more prominent. Horse heart cytochrome C is a globular protein consisting of 104 amino acids, 12 negatively charged (Glu, Asp) and 21 positively charged (Lys, Arg) and characterized by a pI = 10.2. Its molecular weight is 12 384 Da and its shape in aqueous solutions is approximately spherical ($a \times b \times b = 15 \times 17 \times 17$ Å^3). In this study we tune, to some extent, the intermolecular interactions by changing protein concentration, pD and adding two salts differing in the anions. SANS and rheological measurements have been performed on solutions with volume fraction ranging from 0.1 to 0.5 at two different pD (5.4 and 11.0) values. The details of samples composition and preparation are described in the next section.

Experimental section

Material

Cytochrome C from horse heart (product no. C7752) was purchased from Sigma Chemical Company. This product is obtained using a procedure that avoids trichloroacetic acid (TCA), which is known to promote the dimer formation in favor of the native protein.

Two sets of five cytochrome C samples in D_2O at different pD, 5.4 and 11.0, were prepared for SANS and rheological measurements; both of them contain protein volume fraction, ϕ, ranging from 0.1 to 0.5. A list of the sample composition is reported in Table 1. Samples at pD 5.4 were obtained just dissolving cytochrome C in D_2O; those ones at pD 11.0 were prepared adding different volumes of 2 N NaOH/D_2O solution.

Table 1 Cytochrome C sample composition at the two different investigated pD

pD = 5.4 ± 0.1			pD = 11.0 ± 0.1		
ϕ	[p]/mM	I^*/mM	ϕ	[p]/mM	I*/mM
0.100	9.15	—	0.093	8.48	45
0.201	18.35	—	0.198	18.10	95
0.300	27.41	—	0.299	27.33	142
0.400	36.59	—	0.400	36.56	192
0.500	45.72	—	0.496	45.39	238

NaN_3 at a concentration of 0.2 mg ml^{-1} was added to all samples in order to avoid bacterial growth.[16] The ionic strength, I^*, has been calculated considering only the NaOH contribution in the case of pD = 11.0. All the samples were prepared few days before the experiment was performed in order to allow H–D exchange. The same samples have been used for both rheological and SANS measurements.

Methods

Rheological measurements were carried out with a stress-controlled rheometer, Paar Physica Universal Dynamic Spectrometer UDS 200. The experiments have been performed with a 'cone-plate' geometry designed for handling small quantities of sample. To limit the amount of protein needed for the measurement, the cone had a radius 12.5 mm and was placed at 0.05 mm from the plate resulting in a theoretical shear stress range from 0.122 Pa to 36 669 Pa. We performed flow curves varying the shear stress and measuring the shear rate; the viscosity of each point is automatically calculated as the ratio between the preset shear stress and the measured shear rate.

All measurements were carried out at a temperature of 20.0 ± 0.1 °C which was regulated by a controlled peltier system (TEZ 150P) coupled with a Haake circulating bath. The measurements were carried out by imposing a shear stress ranges from 0.22 to 2 Pa or 0.2–15 Pa or 0.2–130 Pa according to the sample viscosity.

Neutron measurements were performed at the NG-7 SANS instrument at the NIST Center for Neutron Research (Gaithersburg, MD) using incident monochromatic neutrons of wavelength $\lambda = 5$ Å with $\Delta\lambda/\lambda = 10\%$.

The sample to detector distance was fixed at 2.5 m, covering the magnitude of scattering vector, Q, from 0.0125 to 0.32 Å^{-1}. The detector was a 65×65 cm^2 ^{3}He position-sensitive proportional counter having a 5×5 mm^2 resolution. The neutron beam on the sample was 1.6 cm in size and circular in shape. The instrumental resolution was taken into account in the model but its effect was negligible since the experimental spectra do not present sharp peaks. Standard (UV) quartz micro-cylindrical cells having a path length equal to 1 mm were used for low viscosity samples. High viscosity samples ($\phi = 0.4$ and 0.5) were contained in titanium demountable cells having two flat quartz windows and being 1 mm in path length. Since the transmission of samples spanned from 90% (for the 0.1 of protein in volume fraction) to about 80% (for the 0.5 of protein in volume fraction) the multiple-scattering effect was not taken into account.

The measured intensity was corrected for background and empty cell contributions, and for non-uniformities in the detector efficiency by dividing data, pixel-by-pixel, by the measured scattering from an isotropic scatterer, such as plexiglass. The data have been rescaled to the absolute intensity by a direct measuring of the beam flux at the sample. The $I(Q)$ *versus* Q data were obtained by a circular average of the so-obtained two-dimensional absolute intensity detector image. The overall data reduction was carried out according to the standard NIST procedures.[19] All the neutron scattering experiments have been performed at $T = 20.0 \pm 0.1$ °C and no condensation of water was present on the quartz cell windows.

Results and discussions

Rheological properties of concentrated cytochrome C solutions have been monitored using steady-state viscosity measurements. Viscosity curves are reported in Figs. 1 and 2 and show the trend of viscosity as a function of the shear rate for all investigated samples. All measurements were performed controlling the shear stress, so that the shear rate range depends on the sample viscosity. Initial experimental values

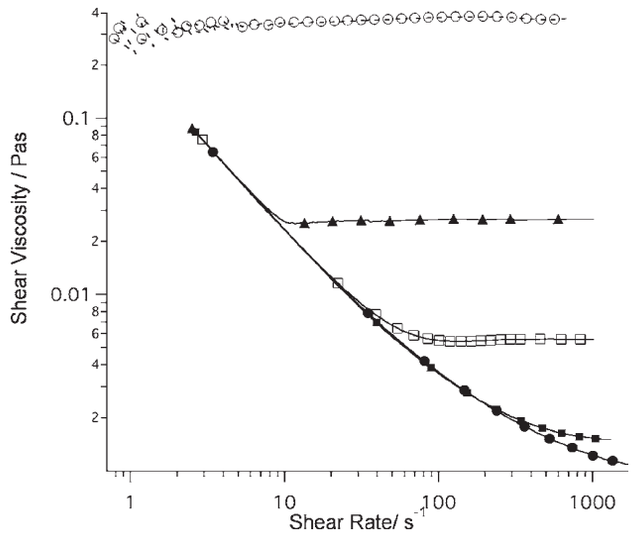

Fig. 1 Experimental shear viscosity is reported as a function of shear rate for samples at pD 5.4 with volume fractions: 0.1 (solid line, full circles, ●); 0.2 (solid line, full squares, ■); 0.3 (solid line, open squares, □); 0.4 (solid line, full triangles, ▲); 0.5 (dash line, open circles, ○).

are 1 s^{-1} in all cases except for the solutions with $\phi = 0.5$ at pD 11.0 and at pD 5.4 where the shear rates start from about 0.05 s^{-1} and 0.5 s^{-1}, respectively.

Rheological behavior of charged colloidal particles has been intensively studied in the case of diluted solutions and three main electroviscous effects have been found.[20] The so-called "primary electroviscous effect" is due to the interactions of the diffuse double layer around each particle; the "secondary electroviscous effect" can be explained in terms of balance of electrostatic repulsive force and hydrodynamic compressive force on each particle; the "tertiary electroviscous effect" is influenced by the particle shape.

A solution of strongly interacting colloidal particles at high volume fractions and low electrolyte concentrations orders into crystalline lattices at rest. If shear is applied, the flow concentrates stress above all at lattice dislocations where particles are loosely trapped. Under flow, the solution's microstructure can be modeled as a 'blend' made up of a solid ordered phase coexisting with a fluid disordered phase and when shear rate increases the disordered phase rises above the ordered one.

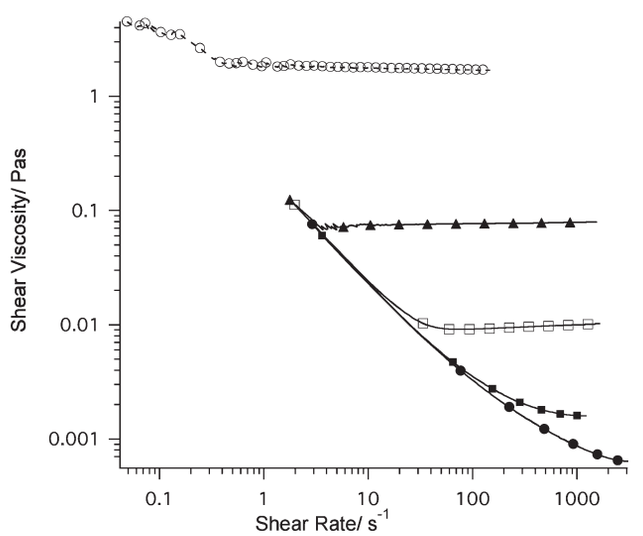

Fig. 2 Experimental shear viscosity is reported as a function of shear rate for samples at pD 11.0 with volume fractions: 0.1 (solid line, full circles, ●); 0.2 (solid line, full squares, ■); 0.3 (solid line, open squares, □); 0.4 (solid line, full triangles, ▲); 0.5 (dash line, open circles, ○).

How exactly these phases are organized is still unclear.[21] The rheological behavior of the solutions we investigated is consistent with this model: the shear leads to a destruction of the ordered structure and the so-called shear-thinning behavior is observed (*i.e.* the shear viscosity decreases as shear rate increases). Usually, pseudo-plastic solutions have a flow curve characterized by three regions with the shear-thinning zone surrounded by two Newtonian plateaus at the edges of the shear rate range.[22,23] Sometimes the low shear Newtonian regions can lie outside the shear rate range accessible to the instrument as in the cases reported in this paper.[24] Unfortunately, due to instrumental limits, the first Newtonian plateau is experimentally detected only for the sample having $\phi = 0.5$ at pD 11.0 since our 'cone-plate' geometry has the intrinsic instrumental lower limit in the shear stress of 0.122 Pa. As expected, the high-shear viscosity exploits a strong concentration dependence increasing with volume fraction and reaching the maximum value in the case of $\phi = 0.5$ at pD = 11.0.

In order to quantitatively describe the flow curves the Sisko approach has been used (eqn. (1)). This relatively simple model[25,26] is useful to describe a shear-thinning behavior in presence of the high shear plateau only:

$$\eta = \eta_\infty + K\dot{\gamma}^{n-1} \quad (1)$$

where K is the consistency index, n is the flow behavior index and η_∞ is the limit viscosity at infinite shear rate. The parameter K gives an indication of the non-Newtonian nature of the sample and can be assimilated to the yield stress in a Bingham-type fluid. When $K = 0$ or $n = 1$, the model describes a simple Newtonian fluid.

The results obtained from the fitting of the experimental data and using the Sisko model are reported in Fig. 3a and the related parameters are listed in Table 2. Only the low concentration cases ($\phi = 0.1$ and 0.2) can be reasonably fitted. The K value turns out to be about 0.2 for all low volume fraction samples, while n gradually decreases, increasing ϕ consistently with a "less Newtonian behavior".

The viscosity curve relative to the sample $\phi = 0.4$ at pD 11.0 almost resembles a Newtonian behavior in the shear rate range we investigated, whereas the sample $\phi = 0.5$ at pD 11.0 behaves more like a pseudo-plastic fluid and two Newtonian regions are detected. This last sample has been fitted using the Cross model[23,25] (Fig. 3b):

$$\eta = \eta_\infty + \frac{\eta_0 - \eta_\infty}{1 + (K\dot{\gamma})^m} \quad (2)$$

where η_0 and η_∞ are the zero shear and the infinite shear viscosities, 4.56 and 1.78 Pa.s, respectively. In the same volume fraction case at pD 5.4 the curve exploits a Newtonian behavior with a viscosity equal to 0.35 Pa.s.

The viscosity trend of samples at high volume fraction can be rationalized in terms of electrostatic charge on the molecules and their aggregation behavior. Electrostatic interactions influence the rheological behavior of solutions: in high concentrated solutions electrostatic interactions overcome Brownian interactions and order occurs, and obviously the electrostatic interactions experienced by the particles depend on their superficial charge.

Generally, in charged systems the viscosity increases with the effective surface charge,[27] but this is not our case. At pD 5.4, molecules have a great positive charge (pI = 10.2) and consequently experience higher electrostatic repulsions with respect to pD = 11.0 where the charge is almost zero, but shear viscosities relative to pD 11.0 are higher than those at pD 5.4. This means that another effect contributes to the rheological behavior of the investigated systems, *i.e.* the aggregation phenomenon is surely favored at pD 11.0 due to the attractive surface of the low charged protein; moreover, this effect enhances with concentration.

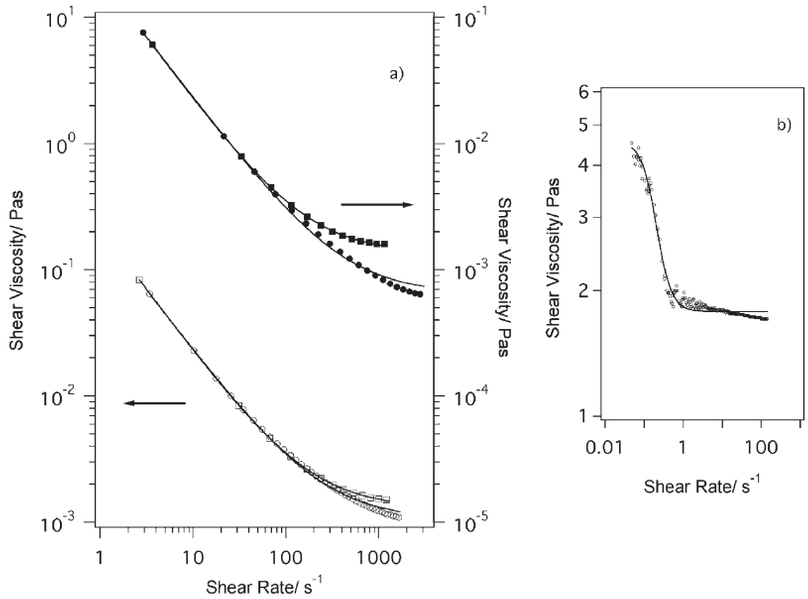

Fig. 3 Shear viscosity as a function of shear rate. (a) Fitted results using Sisko model for samples: pD 11.0 $\phi = 0.1$ (experimental data: full circles, ●, fit data: solid line); pD 11.0 $\phi = 0.2$ (experimental data: full squares, ■, fit data: solid line); pD 5.4 $\phi = 0.1$ (experimental data: open circles, ○, fit data: solid line); pD 5.4 $\phi = 0.2$ (experimental data: open squares, □, fit data: solid line). (b) Fitted results using Cross's model relative to the sample with $\phi = 0.5$ at pD 11.0 (experimental data: open circles, ○, fit data: solid line).

Fig. 4 shows the relative limiting high-shear viscosity, $\eta_{rel} = \eta/\eta_0$, as a function of ϕ both for pD 5.4 and pD 11.0. Rheological behavior of the system can give some insight into the interaction between particles. Furthermore, the strength of the interactions can be estimated varying shear rate conditions. In particular, if an appropriate model can represent the data, the evaluation may be more convenient and effective. Several models have been developed that can be applied to describe the relation between relative viscosity of the samples and volume fraction of the particles in the system.[28] One of the well-known correlations is the Krieger–Dougherty model:

$$\eta_{rel} = \frac{\eta}{\eta_0} = \left(1 + \frac{\phi}{\phi_{max}}\right)^{-[\eta]\phi_{max}} \qquad (3)$$

where the parameters to be fitted $[\eta]$ and ϕ_{max} are the intrinsic viscosity and the volume fraction corresponding to the maximum packing, respectively, while η_0 is the solvent viscosity. Table 3 reports $[\eta]$ and ϕ_{max} at the limit shear-rate and 100 s^{-1}. The maximum packing fraction and the intrinsic viscosity appears to be almost shear-rate independent, increasing shear rate the particles packing is already defined by the repulsive or attractive interaction. At lower shear rates the model is not applicable since all the viscosity curves collapse.

The behavior of the concentrated solution changes from a liquid-like to a solid-like as the volume fraction approaches the maximum packing fraction. Different values have been reported in the literature for the maximum packing fraction of suspensions of monodisperse particles. These results indicate that the maximum packing fraction may change significantly with purity, shape, relative monodispersity of the particles, and the level of accuracy of experiments. Even different models may predict different values for the maximum packing fraction of the same system.

As a reference it is worth to repeat that a system constituted of perfect spheres has an intrinsic viscosity value equal to 2.5 and this value strongly depends on the shape of molecules.[25] The calculated values of $[\eta]$ for cytochrome C concentrated solutions using Krieger–Dougherty model gives much larger values than 2.5. It is known that the intrinsic viscosity of suspensions is affected by the shape and surface roughness of the particles and, since in our system the protein molecules are not exactly spherical, we believe that this may be a reason for the high value of the intrinsic viscosity of the samples. Additionally, the polydispersity of the samples as well as the aggregation may also be responsible for the high intrinsic viscosity. In particular, the deviations from the spherical symmetry cause an increase in magnitude $[\eta]$ that usually ranges from 2.5 (spheres) to 10 (plates). So the obtained values of 5.0 and 5.9, for pD 5.4 and 11.0 respectively, are a reasonable consequence of the ellipsoidal native shape of the cytochrome C mixed with the high complexity of the investigated solutions that involves some sort of aggregation to give more asymmetric structures especially in the case of higher pD confirming

Table 2 Fitting parameters (η_∞,K,n) using the Sisko equation (eqn. (1)) relative to samples with volume fractions 0.1 and 0.2 at pD 5.4 and 11.0

pD	ϕ	η_∞/mPa s	K	n
5.4 ± 0.1	0.100	0.105	0.207	0.035
5.4 ± 0.1	0.201	1.29	0.215	0.01
11.0 ± 0.1	0.093	0.5	0.18	0.1
11.0 ± 0.1	0.198	1.4	0.21	0.005

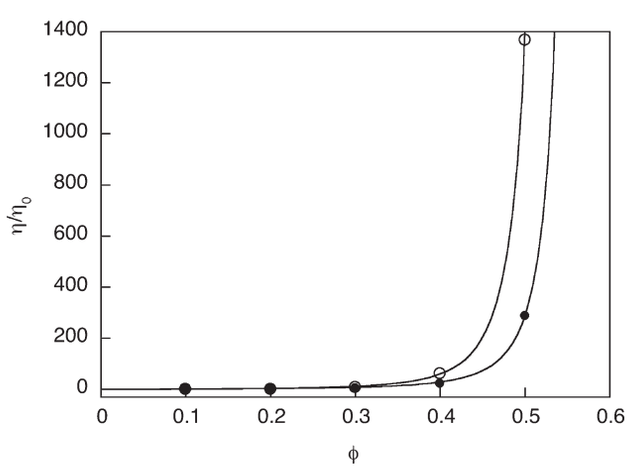

Fig. 4 High shear viscosity as a function of cytochrome C volume fraction: pD = 11.0 (experimental data: open circles, ○, fit curve: solid line), pD = 5.4 (experimental data: full circles, ●, fit curve: solid line).

Table 3 Fitting parameters ($[\eta]$, ϕ_{max}) using the Krieger–Dougherty equation, eqn. (3), relative to the protein samples at pD 5.4 and 11.0 considering the infinite shear-rate limit and shear rate = 100 s^{-1}

	Infinite shear rate limit		Shear rate 100 s^{-1}	
pD	ϕ_{max}	$[\eta]$	ϕ_{max}	$[\eta]$
5.4 ± 0.1	0.584 ± 0.025	5.0 ± 0.4	0.566 ± 0.064	4.6 ± 0.8
11.0 ± 0.1	0.564 ± 0.005	5.9 ± 0.1	0.574 ± 0.020	6.2 ± 0.5

that the aggregation is favored by the low surface charge. Anyway, our sample seems to behave like titanium dioxide suspensions which have $[\eta] = 5.0$ and $\phi_{max} = 0.55$.[29] Moreover, ϕ_{max} values found for the cytochrome C are very similar to those relative to the system of PMMA particles[28] that have been defined as a quasi-hard sphere system.

If we compare the ϕ_{max} values at the two different pD we observe that system at higher pD values is characterized by higher ϕ_{max} values. In particular, the electrostatic interactions become less effective while shear rate increases, so we can conclude that in the high shear rate region excluded volume effects are more effective than electrostatic ones in causing maximum packing values. We anticipate here that addition of salts belonging to the Hofmeister series produces a consistent increase in the intrinsic viscosity with a concomitant appearing of two peaks in the small angle neutron scattering spectra (see below and Fig. 11). We will discuss exhaustively this finding in a forthcoming paper but we can anticipate this is the signature of protein gelation induced by co-ions addition to cytochrome C.

In order to have a deeper insight into the structure, SANS measurements were carried out on all samples. The spectra are showed in Figs. 5 and 6. The main characteristic of these spectra is the maximum in the scattering intensity distribution. Chen *et al.*[16,17] reported similar results, obtained by experiments on cytochrome C in aqueous solutions within a range of volume fractions from 0.05 to 0.18. The presence of a very pronounced interaction peak in the scattering intensity distribution is indicative of local order around macro-ions due to their electrostatic repulsions. In our case, it is evident that at pD 11.0 the peak appears at volume fractions greater than 0.3, that means molecules start interacting at a closer distance. This can be easily explained in term of lower charge on molecules and consequently lower electrostatic potential

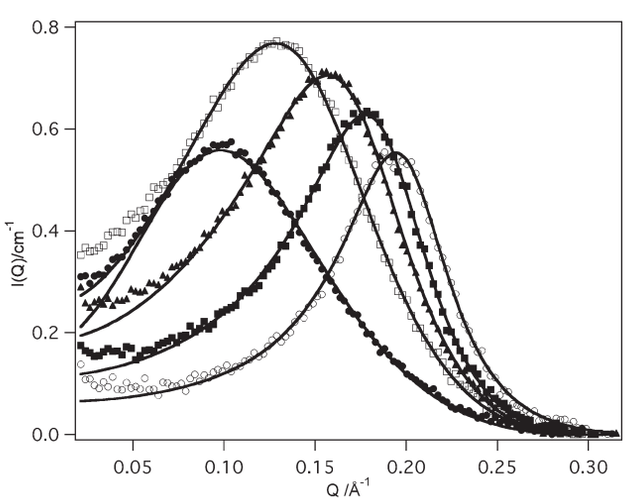

Fig. 5 Experimental and fitted SANS curves atpD 5.4, $\phi = 0.1$ (experimental data: full circles, ●, fit data: solid line); $\phi = 0.2$ (experimental data: open squares, □, fit data: solid line); $\phi = 0.3$ (experimental data: full triangles, ▲, fit data: solid line); $\phi = 0.4$ (experimental data: full squares, ■, fit data: solid line); $\phi = 0.5$ (experimental data: open circles, ○, fit data: solid line).

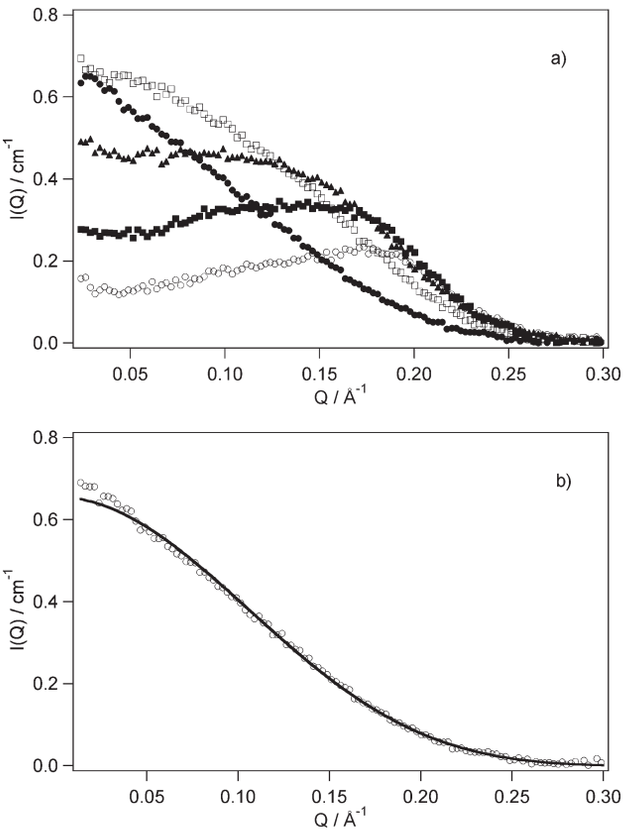

Fig. 6 (a) Experimental scattering intensity distribution as a function of Q for pD 11.0, at volume fraction: 0.1 (full circles, ●); 0.2 (open squares, □); 0.3 (full triangles, ▲); 0.4 (full squares, ■); 0.5 (open circles, ○). (b) Experimental and fitted SANS curves at pD 11.0, $\phi = 0.1$ (experimental data: open circles, ○, fit data: solid line).

experienced since pD 11.0 is very close to the isoelectric point pI = 10.2 and the protein charge very close to zero. Another interesting feature is the concentration dependence of the peak position, Q_{max} as expected. It moves to higher Q values when the volume fraction increases. The peak position can be used to deduce the molecular packing in solutions through a phenomenological approach already used by Chen *et al.* in the case of lithium dodecyl sulfate micellar solutions[30] since it is associated with the reciprocal mean inter-particle distance.

If we assume a face center cubic (fcc) like structure we can calculate the mean intermolecular distance, d, from the protein concentration using the formula:

$$d = \frac{1}{\sqrt{2}} \left(\frac{4000}{N_A[c]} \right)^{1/3} 10^8 \text{ Å} \qquad (4)$$

where N_A is Avogadro's number and [c] is the protein molar concentration. The fcc packing has been chosen in agreement with previous work.[30] This spatial disposition allows all the charged macro-ions to be at the same distance to their first neighbors, while the simple cubic ordering forces some macro-ion to stay closer than others. It is worthy to note that the two dimensional SANS images did not show any diffraction peak in agreement with a globally disordered sample.

In Fig. 7 we report $Q_{max}d$ as a function of d; the values we used are listed in Table 4. The linear trends obtained are respectively:

$$Q_{max}d = 8.434\text{–}0.0334d \quad \text{at} \quad \text{pD} = 5.4$$

$$Q_{max}d = 16.975\text{–}0.2869d \quad \text{at} \quad \text{pD} = 11.0$$

They are in agreement with previous literature results and confirm the hypothesis that the increased volume fraction generates a high packing structure, following in this case an fcc

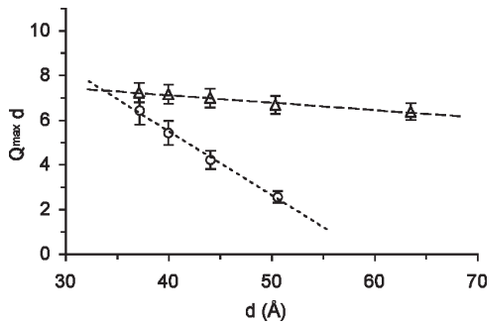

Fig. 7 $Q_{max}d$ as a function of d: pD = 11.0 (open circles, ○) y = −0.2869x + 16.975; pD = 5.4 (open triangles, △) $y = -0.0334x + 8.4336$.

disposition. It must be underlined that these two curves cross at about 33 Å, which is the protein diameter. It is essential to point out that this phenomenological approach is not accurate and only qualitatively describes the packing process induced by the increase in volume fraction since the interaction peaks coming from the spectra are not Bragg peaks.

In order to fit the experimental data quantitatively we used the following equation:

$$I(Q) = A_p P(Q) S(Q) \tag{5}$$

where A_p is the amplitude factor. In the case of a globular protein cytochrome C, it is given by:

$$10^{-3}[\mathrm{p}]N_\mathrm{A}[b_{pa} + N_\mathrm{ex}(b_\mathrm{D} - b_\mathrm{H})\chi + mb_\mathrm{solv} - V_\mathrm{H}b_\mathrm{solv}/v_\omega]^2 \tag{6}$$

where N_A is Avogadro's number, [p] the protein concentration in mM, $b_{pa} = \sum_p b_i = 258.5164 \times 10^{-12}$ cm the total scattering length of the protein, N_ex the number of labile protons that the protein can exchange with the solvent, b_H and b_D are respectively the scattering length of the hydrogen and deuterium, m is the number of solvent molecules in the hydration shell, V_H is the hydrated protein volume, $v_\omega = 30$ Å^3 is the volume of a water molecule, b_solv is the solvent scattering length calculated each time according to the sample composition using the formula $b_\mathrm{solv} = \chi b_{D_2O} + (1-\chi)b_{H_2O}$ where χ is the volume fraction of D_2O in the solvent and b_{D_2O} and b_{H_2O} are respectively the D_2O and H_2O scattering length. All these parameters are known, in particular the amount of H/D exchange of the protein in D_2O heavy water-containing solvents and the hydration have been experimentally obtained through contrast variation measurements:[16] $N_\mathrm{ex} = 165$ and $m = 112$.

The $P(Q)$ is the normalized form factor for a core-shell oblate ellipsoid ($a \times b \times b$) having the axis ratio, $a/b = 0.88235$, in agreement with previously published results[16] and assuming the presence of an hydration shell coming from the adsorption of water molecules at the protein surface. The protein structure factor, $S(Q)$, has been determined according to the generalized one-component macro-ion model (GOCM) already tested.[30] As said above the GOCM extends the OCM based on DLVO interaction, which is valid only in dilute solutions, to finite macro-ion concentrations. A protein solution is described as made up of charged macro-ions experiencing screened Coulomb interaction.

In order to calculate the scattering length densities we assumed that a protein in solution to be consisted of a uniform core surrounded by (about 20% of the protein) a hydrated outer shell.

Hence the parameters free to change are the major core axis b, the charge, the background and the volume fraction.

In the case of pD = 5.4 the described model works well with the experimental spectra up to a volume fraction of 0.4. At greater volume fractions the model fails in the determination of the protein charge, Z. In particular, we obtained a mean value of the major axis of 16.0 ± 1.5 Å with a core major axis of 14.0 ± 1.5 Å and the protein charge is about 4.5 ± 0.5 (Table 5) for all volume fractions with the exception of $\phi = 0.5$ where the consistently high value of 10.5 is obtained. This could be due to the fact that a short-range attractive interaction becomes important when the protein molecules are forced to partially overlap. This extra contribution is not taken into account by the electrostatic potential that describes $S(Q)$ (see Fig. 5 and Table 5 and in particular note that the peak at $\phi = 0.5$ is by far sharper than the other lower volume fraction cases, 0.1–0.4).

Table 4 Q_{max} and d values relative to samples at pD = 5.4 and pD 11.0

ϕ	Q_{max}/Å^{-1}	d/Å
pD 5.4 ± 0.1		
0.100	0.100	63.6
0.201	0.132	50.4
0.300	0.158	44.1
0.400	0.178	40.0
0.500	0.194	37.2
pD 11.0 ± 0.1		
0.093	—	65.2
0.198	0.050	50.6
0.299	0.095	44.1
0.400	0.135	40.0
0.496	0.172	37.3

Table 5 Fitting results using the GOCM model relative to samples at pD 5.4. SLD = scattering length density

pD = 5.4 ± 0.1					
Volume fraction	0.100	0.201	0.300	0.400	0.500
Core major axis/Å	15.2	15.2	14.4	13.7	13.3
Shell/Å	1.5	1.3	2.3	2.7	2.2
10^6 SLD core/Å^{-2}	2.906	2.906	2.906	2.906	2.906
10^6 SLD shell/Å^{-2}	5.249	5.161	5.055	4.919	4.743
10^6 SLD solvent/Å^{-2}	6.286	6.160	6.007	5.811	5.557
Charge	4.4	4.7	4.6	4.7	10.5
I^*/M	0	0	0	0	0
B/kg cm^{-1}	0.131	0.227	0.268	0.344	0.468

Table 6 Fitting results using the GOCM model relative to samples at pD 11.0. SLD = scattering length density

pD = 11.0 ± 0.1	
Volume fraction	0.093
Core major axis/Å	12.40
Shell/Å	5.5
10^6 SLD core/Å^{-2}	2.906
10^6 SLD shell/Å^{-2}	5.250
10^6 SLD solvent/Å^{-2}	6.288
Charge	—
I*/M	—
B/kg cm^{-1}	0.1194

Table 7 pK_a values of protein residues[31]

	N term	Arg	Asp	Glu	His	Lys	Lys	Tyr	C term	Heme A	Heme D
pk_a	9.60	14.50	1.00	3.36	6.50	12.40	10.50	10.00	−1.40	2.10	3.00
# a.a.	1	2	3	9	2	11	8	4	1	1	1

The theoretical protein charge value calculated through the pK_a values of protein residues[31] is about 8.9 and is higher than the one we reported (see Table 7). In order to explain such a result, we must invoke the so-called charge renormalization phenomenon.[17] The protein charge reported in the tables is an interaction charge and not the actual charge on the protein surface. The interaction charge is the charge really experienced by protein and it is the surface charge due to the ionization of external residues reduced by the counter ions that adsorb at interface and are part of the protein itself.

Concerning samples at pD 5.4 we calculated the structure and form factor using the GOCM model and Figs. 8 and 9 show the trend of $S(Q)$ and $P(Q)$, respectively. We can note that going from $\phi = 0.1$ to 0.5 the first interaction peak moves at higher Q values and its intensity increases. Besides, $S(Q \rightarrow 0)$ reduces on raising the protein concentration.

In the case of pD 11.0 the experimental scattering curve relative to $\phi = 0.1$ was fitted using only the ellipsoidal form factor (see Fig. 6b and Table 6). The protein at pD 11.0 and $\phi = 0.1$ presents a negligible inter-particle interactions. Unfortunately, the only form factor approach and the GOCM model fail to describe volume fractions higher than 0.1. At this pD, the protein charge is low and some other effects, different from the electrostatic one, dominate the intermolecular potential and are not considered in the description. A new theoretical framework is under development in order to account the short-range attraction potential and will be the subject of a forthcoming paper.

As at this pD we were unable to extract the $S(Q)$ through GOCM, we estimated an "experimental structure factor" $S'(Q)$, obtained by dividing the scattering intensity distribution, $I(Q)$, by the form factor, $P(Q)$, obtained from the fitting of data at $\phi = 0.1$ (see Fig. 6b). These experimental structure factors are shown in Fig. 10. They look qualitatively different from the structure factors at pD = 5.4 shown in Fig. 8.

SANS experiments were also performed on protein solutions with volume fractions 0.3, 0.4 and 0.5 at pD = 11.0, in the presence of NaCl and NaSCN in a range of concentrations from 0.1 M to 2.8 M. In some of these samples we detected the presence of a second interaction peak at small Q values. As an example, Fig. 11 shows the SANS spectra taken at the protein volume fraction 0.4 with the presence of NaCl and NaSCN at concentrations 1.9 and 1.2 M, respectively. The presence of the second peak is clearly due to a protein cluster formation favored by the screening of the protein charge and the appearance of an attractive force induced by salt, and can be considered as the signature of the gelation process. Fig. 11 emphasizes clear evidence that both the position and magnitude of the "cluster related" peak are affected by both the concentration and the nature of the salt anion. In particular, a lower concentration of NaSCN causes a stronger cluster formation (the peak position in Q at 0.05 $Å^{-1}$ instead of 0.1 $Å^{-1}$ in the presence of NaCl, along with a higher amplitude of the peak. The stronger NaSCN effect can be related to the well-known Hofmeister effect.[6] A quantitative description of the gelation process is in progress and will be reported in a forthcoming paper.

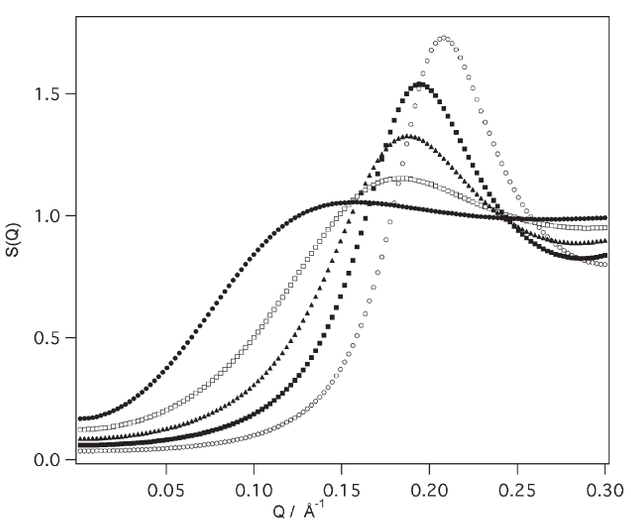

Fig. 8 Fitted $S(Q)$ curves at pD 5.4, $\phi = 0.1$ (full circles, ●); $\phi = 0.2$ (open squares, □); $\phi = 0.3$ (full triangles, ▲); $\phi = 0.4$ (full squares, ■); $\phi = 0.5$ (open circles, ○).

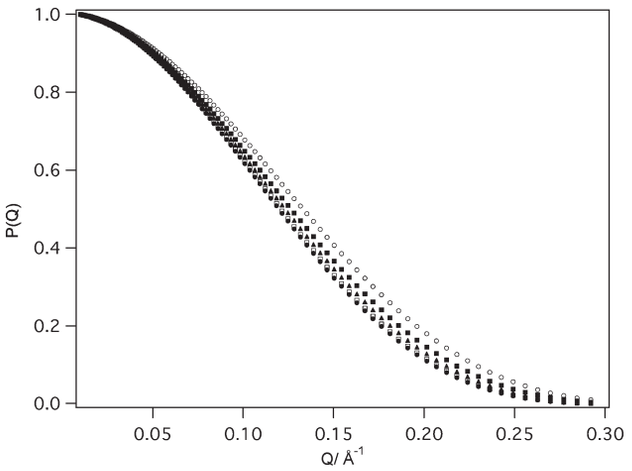

Fig. 9 Fitted $P(Q)$ curves at pD 5.4, $\phi = 0.1$ (full circles, ●); $\phi = 0.2$ (open squares, □); $\phi = 0.3$ (full triangles, ▲); $\phi = 0.4$ (full squares, ■); $\phi = 0.5$ (open circles, ○).

Conclusions

In this paper we studied the pD and concentration effect on the intermolecular interactions among cytochrome C molecules using small angle neutron scattering and rheological experiments. The concentration effect is quite obvious: increasing the number of molecules per unit volume, the protein macroions are forced to stay closer generating a stronger interaction potential. This is confirmed both by the position of the interaction peak in the SANS intensity distribution and by the increase in viscosity of the sample. It is well known that the surface charge on proteins and consequently their mutual interactions depend on the H^+ concentration in solution. Two pD values were chosen in such a way that a strongly positive charged situation was compared with a weakly negatively charged one, both with the protein in the native state.

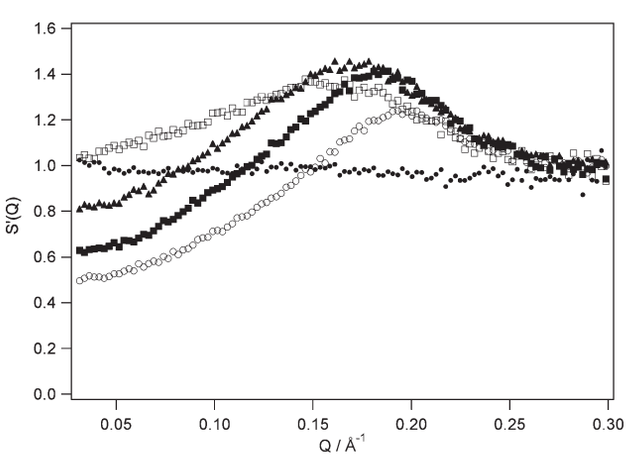

Fig. 10 'Experimental' $S'(Q)$ curves at pD 11.0, $\phi = 0.1$ (full circles, ●); $\phi = 0.2$ (open squares, □); $\phi = 0.3$ (full triangles, ▲); $\phi = 0.4$ (full squares, ■); $\phi = 0.5$ (open circles, ○).

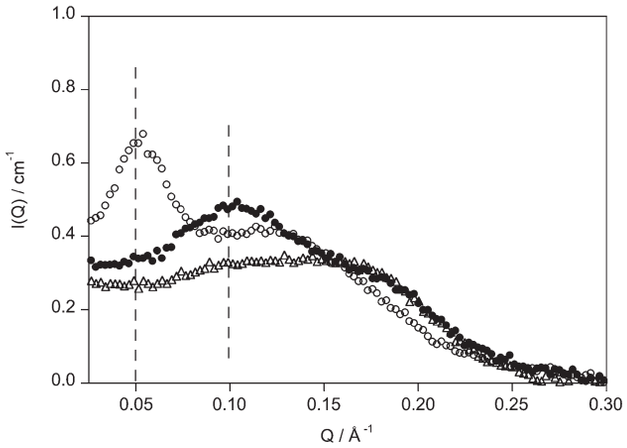

Fig. 11 Experimental scattering intensity distribution as a function of Q for pD = 11.0 and at volume fraction 0.4: the spectrum taken without salt added has only one interaction peak present (open triangles, △); while the spectra with addition of salt are characterized by the presence of two peaks, a low Q peak typical of a gel structure and a higher Q peak due to the protein globule. 1.9 M NaCl (full circles, ●); 1.2 M NaSCN (open circles, ○).

The SANS spectra at pD = 5.4 were fitted using the GOCM and a good agreement between the theory and experiments up to a volume fraction of 0.4 was shown. At pD = 11.0, the spectrum at $\phi = 0.1$ is a pure form factor (oblate ellipsoid). We found that at pD = 5.4 and for volume fraction of 0.5 and for all volume fractions at pD = 11.0 the GOCM fails. This is probably due to the presence of some attractive contribution in the interaction potential that the GOCM does not take into account. This part of the potential becomes effective at high concentration of charged molecules ($\phi = 0.5$ and pD = 5.4) and for volume fractions higher than 0.1 in the case of uncharged molecules (pD = 11.0). The main consequence of this attractive interaction is the occurrence of an aggregation phenomenon also confirmed through rheological measurements. Viscosity values at pD = 11.0 are higher than those at pD 5.4 in contrast with the usual findings that the higher the surface charge the higher the viscosity. So the trend of high shear viscosity as function of concentration and pD as well as the maximum packing values can be rationalized only by invoking an attractive interaction among proteins that overcomes the standard coulombic repulsion. The behavior of high concentrate protein solutions in the presence of salt belonging to the Hofmeister series is reported. Addition of salt induces the transformation from liquid to a gel. This is a result of formation of ordered fractal clusters as is evident from appearance of a second interaction peak at very low Q (magnitude of the scattering vector). The appearance of the low Q peak that is also accompanied by a strong increase in the relative viscosity can be considered as *the signature of the gelation process*.

Acknowledgements

Authors express their thanks to C. J. Glinka (NCNR, Gaithersburg) for help with the experimental setup and to the NIST Center for Neutron Research (NCNR, Gaithersburg) for allocating neutron beam time at NG7-SANS spectrometer. Research of SHC is supported by a grant from Materials Research Program of US DOE. Finally, B.L., E.F. and P.B. acknowledge MIUR (PRIN-2003 grant) and the Consorzio Interuniversitario per lo Sviluppo dei Sistemi a Grande Interfase (CSGI, Florence, Italy) for partial financial support.

References

1 L. J. DeLucas and C. E. Bugg, *Trends Biotechnol.*, 1987, **5**, 188.
2 P. Weber, *Advances in protein chemistry*, ed. C. B. Afinsen, F. M. Richards, T. J. Edsal and D. S. Eisenberg, Academic Press, New York, 1991.
3 *Crystallization of Nucleic Acids and Proteins: a Practical Approach*, ed. A. Ducruix and R. Giege, Oxford University Press, 1992.
4 A. A. Chernov and H. Komatsu, *Science and Technology of Crystal Growth*, ed. J. P. V. d. Eerden and O. S. L. Bruinsma, Kluwer, 1995.
5 N. J. Darby and T. E. Creighton, *Protein Structure*, Oxford University Press, Oxford, 1993.
6 F. Hofmeister, *Arch. Exp. Pathol. Pharmakol. (Leipzig)*, 247, **24**, 1888.
7 A. George and W. W. Wilson, *Acta Crystallogr. D*, 1994, **D50**, 361.
8 M. Muschol and F. Rosenberger, *J. Chem. Phys.*, 1995, **103**, 10 424.
9 M. Muschol and F. Rosenberger, *J. Cryst. Growth*, 1996, **167**, 738.
10 M. Muschol and F. Rosenberger, *J. Chem. Phys.*, 1997, **107**, 1953.
11 B. V. Derjaguin and L. Landau, *Acta Physicochim. URSS*, 1941, **14**, 633.
12 E. J. Verwey and J. T. G. Overbeek, *Theory of the Stability of Lyophobic Colloids*, Elsevier, Amsterdam, 1948.
13 R. Piazza, *J. Cryst. Growth*, 1999, **196**, 415.
14 R. Piazza, V. Peyre and V. Degiorgio, *Phys. Rev. E*, 1998, **58**, R2733.
15 D. F. Rosenbaum and C. F. Zukoski, *J. Cryst. Growth*, 1996, **169**, 752.
16 C.-F. Wu and S. -H. Chen, *J. Chem. Phys.*, 1987, **87**, 6199.
17 C.-F. Wu and S.-H. Chen, *Biopolymers*, 1988, **27**, 1065.
18 J. B. Hayter and J. Penfold, *Mol. Phys.*, 1981, **46**, 651.
19 http://www.ncnr.nist.gov/programs/sans/manuals/data_red.html.
20 W. B. Russel, *J. Fluid Mech.*, 1979, 401.
21 B. van der Vorst, D. van den Ende, N. J. J. Aelmans and J. Mellema, *Phys. Rev. E*, 1997, **56**, 3119.
22 S. Chynoweth and Y. Michopoulos, *J. Non-Newton. Fluid. Mech.*, 1997, **69**, 1.
23 G. P. Roberts, H. A. Barnes and P. Carew, *Chem. Eng. Sci.*, 2001, **56**, 5617.
24 A. Lazaridou, C. G. Biliaderis and M. S. Izydorczyk, *Food Hydrocolloids*, 2003, **17**, 693.
25 H. A. Barnes, J. F. Hutton and K. Walters, *An Introduction to Rheology*, Elsevier Science Publishers B. V., Amsterdam, 1989.
26 N. Kiratzis and P. F. Luckham, *J. Eur. Ceram. Soc.*, 1998, **8**, 783.
27 F. M. Horn and W. Richtering, *J. Rheol.*, 2000, **44**, 1279.
28 J. W. Goodwin and R. W. Hughes, *Rheology for Chemists – An introduction*, Royal Society of Chemistry, Cambridge, 2000.
29 R. Turian and T. F. Yuan, *Alche J.*, 1977, **23**, 232.
30 S.-H. Chen and E. Y. Sheu, in *Micellar Solutions and Microemulsions*, ed. S.-H. Chen and R. Rajagopalan, 1990.
31 H.-X. Zhou and M. Vijayakumar, *J. Mol. Biol.*, 1997, **267**, 1002.